Spatial and temporal variability of freezing level in Patagonia's atmosphere.

Nicolás García-Lee[1], Claudio Bravo[1], Álvaro Gónzales-Reyes[2,3,4,5], Piero Mardones[6]

[1]Glaciología y Cambio Climático, Centro de Estudios Científicos (CECs), Valdivia, 5090000, Chile.
[2]Instituto de Ciencias de la Tierra (ICT), Facultad de Ciencias, Universidad Austral de Chile, Valdivia 5090000, Chile.
[3]Laboratorio de Dendrocronología y Cambio Global, Universidad Austral de Chile, Valdivia, 5090000, Chile.
[4]Centro de Humedales Río Cruces (CEHUM), Universidad Austral de Chile, Valdivia, 5090000, Chile
[5]Centro de Investigación, Dinámica de Ecosistemas Marinos de Altas Latitudes (IDEAL), Universidad Austral de Chile, Valdivia, 5090000, Chile.
[6]Centro de Investigación en Ecosistemas de la Patagonia (CIEP), Coyhaique, 5950000, Chile.

Correspondence to: *Nicolás D. García Lee* (ngarcia@cecs.cl)

Abstract. The height of the 0°C isotherm (H_0), commonly signals the freezing level, denotes the lowest height within a specific location's atmosphere where the air temperature reaches 0°C. This can be used as an indicator for the transition between rain and snow, making it useful for monitoring and visualizing the height of freezing temperatures in the atmosphere. We study the spatial and temporal variability of H_0 across Patagonia (41°-54°S) for the 1959-2021 period using reanalysis data from ERA5. Our results indicate that the average isotherm in Patagonia is at 1691 meters above sea level (m a.s.l). The spatial distribution of the annual mean field highlights the contrast in the region, with average maximum of 2658 m a.s.l in the north and minimum of 913 m a.s.l in the south. Regarding seasonal variability in the region, H_0 ranges from 575 m a.s.l (winter) to 3346 m a.s.l (summer). Further, the significant trends calculated over the period show positive values in the whole area. This indicates an upward annual trend in the H_0, between 8.8 and 36.5 meters per decade from 1959-2021, being the higher value in northwestern Patagonia. These upward trends are stronger during summer (8-61 m/decade). Empirical orthogonal function (EOF) analysis was performed on H_0 anomalies. The first empirical orthogonal function (EOF) mode of H_0 variability accounts for 84% of the total variance, depicting a monopole structure centred in the northwest area. This mode exhibits a strong and significant correlation with the spatial average H_0 anomalies field (r=0.85), the Southern Annular Mode (SAM, r=0.58), temperature at 850 hPa in the Drake Passage (r=0.56), and sea surface temperature off the western coast of Patagonia (r=0.66); underscoring the significant role of these factors in influencing the vertical temperature profile within the region. The spatial distribution of the second (8%) and third (4.4%) EOF modes depict a dipole pattern, offering additional insights into the processes influencing the 0°C isotherm, especially on the western slope of Patagonia.

1 Introduction

Patagonia, situated in the southern region of South America, is renowned for its distinct meteorological conditions and glaciers moulded by its geographical features (Aravena & Luckman, 2009; Bravo et al., 2021; Masiokas et al., 2020; Sauter, 2020). Spanning approximately from 40°S to 55°S, the austral Andes, reaching heights of around 1500 m a.s.l., act as an obstacle that hinders the progress of moist tropospheric air masses originating from prevailing westerly winds (Garreaud et al., 2009).

The presence of this geographical barrier, along with the occurrence of baroclinic eddies, strong winds, and the influence of the Pacific Ocean, generates a significant climatic distinction between the western and eastern areas of Patagonia, leading to a pronounced precipitation gradient (Carrasco et al., 2002; Garreaud et al., 2013). These effects are mainly driven by the orographic ascent expansion and cooling of the air on the windward side. While in leeward precipitation is inhibited as descending air heats up and any lingering liquid water evaporates (Lenaerts et al., 2014; Roe, 2004; Siler et al., 2013). Consequently, the western slopes receive substantial precipitation exceeds 5000 mm/year, fostering the growth of lush rainforests, rivers, and numerous glaciers. Conversely, the eastern slope exhibits a semi-arid steppe climate with a rain-shadow effect, receiving less than 1000 mm/year of precipitation (Garreaud et al, 2013; Lenaerts et al., 2014).

The climate of Patagonia is strongly influenced by modes of variability, where the Southern Annular Mode (SAM) is the primary driver of extratropical climate variability in the Southern Hemisphere (Marshall 2003; King et al., 2023; Thomas et al., 2017; Hao et al., 2017). The SAM significantly affects the westerly flow, shaping the atmospheric circulation patterns in the region. It is characterized by an equivalent barotropic, longitudinally symmetric structure that involves a mass exchange between the mid and high latitudes (Garreaud et al., 2009). The SAM strengthens and shifts the polar jet stream poleward during its positive phase. This intensifies the westerly flow, leading to notable changes in temperature and precipitation patterns across Patagonia. Conversely, during its negative phase, the SAM weakens and shifts the polar jet stream equatorward, impacting atmospheric circulation and influencing the region's climate. As a result, the variations in the SAM play a crucial role in modulating the westerly flow and have significant implications. The circumpolar anomalies in westerly flow and tropospheric temperature observed during each phase of SAM result in corresponding anomalies in precipitation and surface temperature in Patagonia (Carrasco-Escaff et al., 2023). In the positive phase, higher temperatures and intensified westerly winds toward higher latitudes (Bravo et al., 2019; Fogt & Marshall, 2020). Conversely, the negative phase of the SAM produces contrasting effects. During the latter half of the 20th century, the SAM exhibited a positive trend, potentially influenced by anthropogenic factors (ozone depletion and increase of greenhouse gases), which could have implications for future climatic (Abram et al., 2014; Fogt & Marshall, 2020).

Carrasco-Escaff et al. (2023), elucidate another key atmospheric system in the region, called the "Drake Low", which exhibits anomalies in cyclonic circulation around the Drake Passage. These anomalies extend longitudinally from the Amundsen Sea to the northeastern part of the Antarctic Peninsula and latitudinally from the western Antarctic coast to the southernmost tip of

South America (designated as R1 area). The presence of the Drake Low intensifies westerly winds, which notably affects the Patagonian region. This intricate system operates through a thermodynamic mechanism facilitated by a core of cold air, playing an active role in cooling the Patagonian region during the summer months. The study's findings provide valuable insights into the complex interplay between large-scale atmospheric dynamics and their direct influence on regional climate patterns.

Revisiting the distinctive attributes of the region, the Northern and Southern Patagonian Icefields, which encompass the largest glacier area in Patagonia, play an important role in the local and regional environment (Dussaillant et al., 2012). Recent research underscores their significant contribution to the rise in sea level compared to other ice masses in South America (Malz et al., 2018; Masiokas et al., 2020; Minowa et al., 2021), and the increasing loss of mass over the past few decades (Hugonnet et al., 2021). The sustained in atmospheric warming has a profound impact on the mass balance of glaciers (Van der Geest & Van den Berg, 2021), especially in terms of the 0°C isotherm (Schauwecker et al., 2017). Changes in this variable results in changes in the snow accumulation rates, amplified melting, and heightened flow rates during moderate or extreme precipitation events, such as atmospheric rivers (Saavedra et al., 2020). This, in turn, renders the region more susceptible to natural hazards, including an increased risk of floods (Somos-Valenzuela et al., 2020), landslides, and Glacial Lake Outburst Floods (Iribarren-Anacona et al., 2015; Mardones & Garreaud, 2020). Nonetheless, the limited availability of data and analysis (particularly at the highest elevations) has hindered our comprehensive understanding of the fundamental mechanisms governing the interaction between these variables and the freezing level, especially the large-scale climate processes operating on different timescales.

This study aims to assess and quantify the patterns and variations of isotherm 0°C in Patagonia. In the first section, we estimated the freezing level values based on ERA5 reanalysis data (climate-grided product), which were subsequently validated with observed data from 4 radiosonde stations. Next, we analysed spatial pattern, seasonal and annual cycles, trend, and interannual variability using reanalysis data from 1959-2021. The discussion section addresses the reanalysis limitations, spatial-temporal distribution, large-scale drivers, and their implications.

2 Data and Methods

2.1 Study Area

Our research focuses on a vast expanse of Patagonia, delineated by a red rectangle in Figure 1a. This region spans latitudes from 41° to 54°S and longitudes from 78° to 66°W, encompassing small fractions of both the Pacific and Atlantic Oceans. The selection of this domain was guided by the locations of radiosonde stations, specifically Puerto Montt (northwest, at 84 m a.s.l), Comodoro Rivadavia (northeast, at 58 m a.s.l), Río Gallegos (southeast, at 20 m a.s.l), and Punta Arenas (south, at 38 m a.s.l). Despite potential limitations posed to the west by Puerto Montt station (as a border domain point), we extended the area towards the west (78°W) to include a significant portion of western Patagonia and the Pacific coast. Moreover, this longitudinal range encompasses the austral Andes (AA) and the glaciers of the Northern and Southern Patagonia Ice Field.

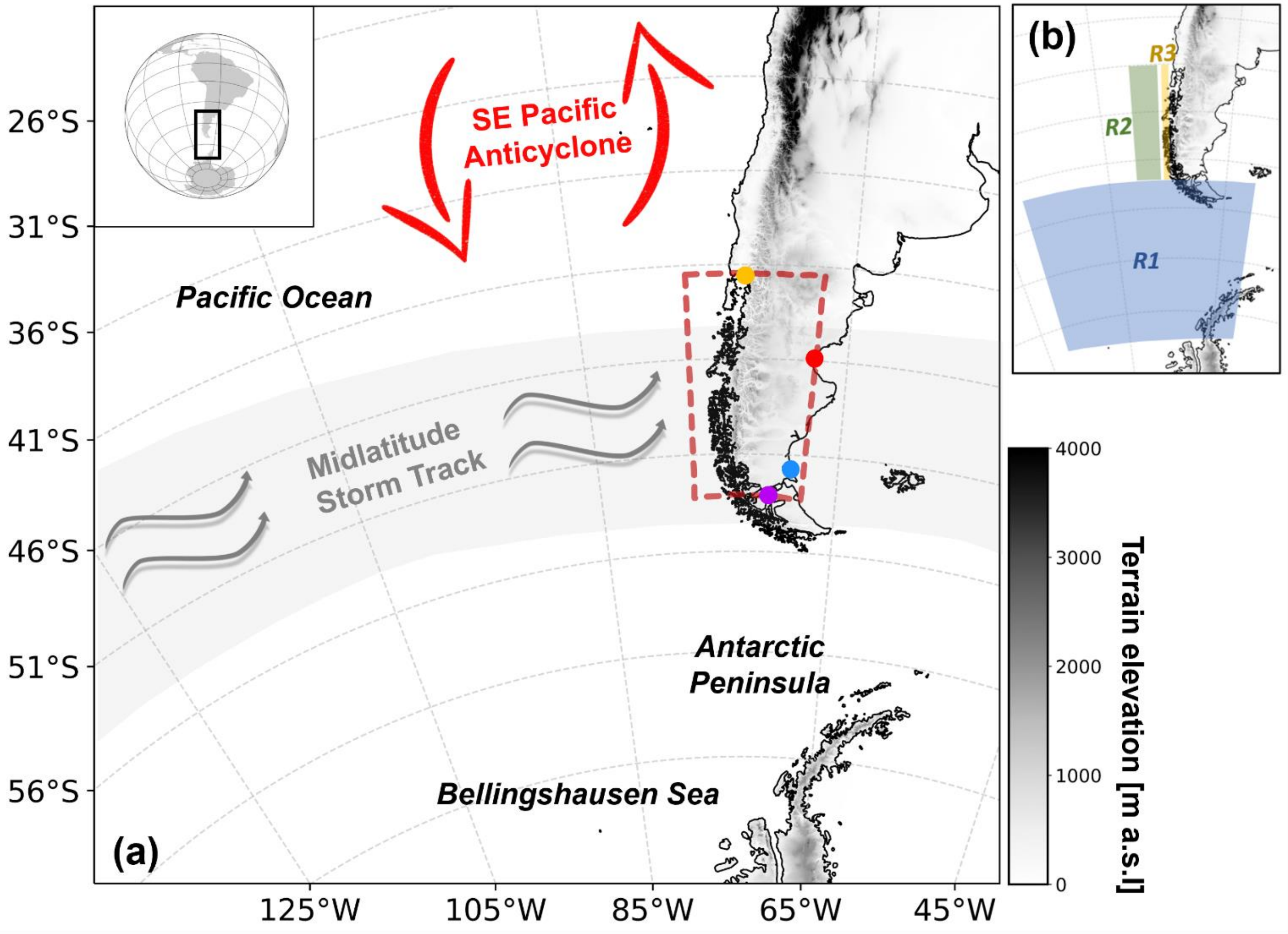

Figure 1: a) Topographic map of South America highlighting key features in the Patagonia region. Terrain elevation (m a.s.l) acquired from ETOPO1 model with 1 arcmin resolution. The red rectangle indicates the study region of Patagonia. The dots indicate the locations of the radiosonde stations of Puerto Montt (orange), Comodoro Rivadavia (red), Río Gallegos (blue), and Punta Arenas (purple). b) Coloured areas represent the regions used for the construction of custom climate indices.

2.2 Assessment of isotherm at 0°C

Two sets of data were used to estimate the free tropospheric values of the 0°C isotherm. The first corresponds to ERA5 reanalysis data (Hersbach et al., 2020). This reanalysis comprises a latitude-longitude grid with a spatial resolution of 0.25°x0.25°, encompassing 37 pressure levels. For our analysis, we utilize the hourly data from 1959 to 2021. Then, we extract vertical profiles of air temperature and geopotential height, spanning levels from the surface up to 400 hPa. Each profile is analysed to identify the temperature transition above and below 0°C. ERA5 freezing levels values (H_0^{ERA5}) are determined by linear interpolation between the geopotential heights corresponding to the transition levels. If multiple elevations of zero degrees are found, for instance, from temperature inversions, the lowest value is assigned. Additionally, if no zero crossing levels are found, the corresponding value is flagged as missing. To obtain a representative value per day, we calculate the daily average of H_0^{ERA5} (H_0-Daily average, Figure 2) using five values (00, 06, 12, 18, 24 UTC). This approach ensures that we capture the diurnal variability and provide a comprehensive picture of the freezing level throughout the day. We utilized a second dataset comprising observations from radiosonde stations. We applied the proposed methodology to estimate the radiosonde freezing levels values (H_0^{IGRA}), allowing us to validate the freezing level values obtained from ERA5 at specific locations. These observed values were obtained from the Integrated Global Radiosonde Archive (IGRA) product (Durre et al., 2018). With this data, we implemented an additional criterion, specifically utilizing vertical profiles that included a minimum of 3 data points. Vertical profiles with inadequate data were excluded from the analysis. Fourth locations with comparable recording periods were selected for analysis: Puerto Montt, Comodoro Rivadavia, Río Gallegos and Punta Arenas (Figure 1). The selection criteria for these locations were established to include only those with a minimum of a decade's worth of data, excluding other locations that do not meet this criterion. We compared the grid's closest point of H_0^{ERA5} to the H_0^{IGRA} and only 12Z data was used to assess their agreement between them. Only this hour was selected since it has a greater number of observations in the records. The outcomes of this process are summarized in Table 1, where Pearson correlation, root mean square error (RMSE), standard deviation and average were estimated in selected periods for each location.

2.3 Indices and Trends

To analyse large-scale patterns associated with $\mathbf{H_0}$, we followed the methodology of the NOAA Climate Prediction Center (https://www.cpc.ncep.noaa.gov/products/precip/CWlink/daily_ao_index/history/method.shtml, last access: 10 January 2024.) to construct the SAM index. This index is derived by projecting 700 hPa geopotential height anomalies onto the loading pattern of the SAM, which is defined as the leading empirical orthogonal function (EOF 1) of monthly mean at the 700 hPa geopotential height anomalies from 20°S poleward during the period 1959-2021 (Shi et al., 2019). For more details check Teleconnection Pattern Calculation Procedures from NOAA’s Climate Prediction Center (CPC) (https://www.cpc.ncep.noaa.gov/products/precip/CWlink/daily_ao_index/history/method.shtml, last access: 10 January 2024.). Anomalies are computed relative to the corresponding month's mean over the same period. To ensure equal area weighting in the covariance matrix, the gridded data is weighted by the square root of the cosine of latitude. Besides, we performed spatial averaging of monthly ERA5 values for specific areas and variables, following the methodology outlined by Carrasco-Escaff et al. (2023), with the exception that we use standardized indices. In Figure 1b, the R1 box represented the geopotential height at 300 hPa and air temperature at 850 hPa near the Drake Passage (68-53°S and 100-60°W). The R2 box represented the southeast Pacific SST adjacent to central Patagonia (52.5-41°S and 80-76°W). Lastly, the R3 box represented the zonal wind at 850 hPa impacting central Patagonia (52.5-41°S and 75.5-74.5°W). These time series were labelled as R1-

Z300, R1-T850, R2-SST, and R3-U850, respectively. Our objective is to comprehend the similarities and influences that these regions and variables may exert on the temperature profile within the area. Trend values of H_0 are estimated, which are derived from the Mann-Kendall test and Theil-Sen estimator (Wilks, 2019; Hussain et al., 2019). A trend was considered statistically significant if the p-value < 0.05. A summarized scheme of the methodology implemented is presented in Figure 2.

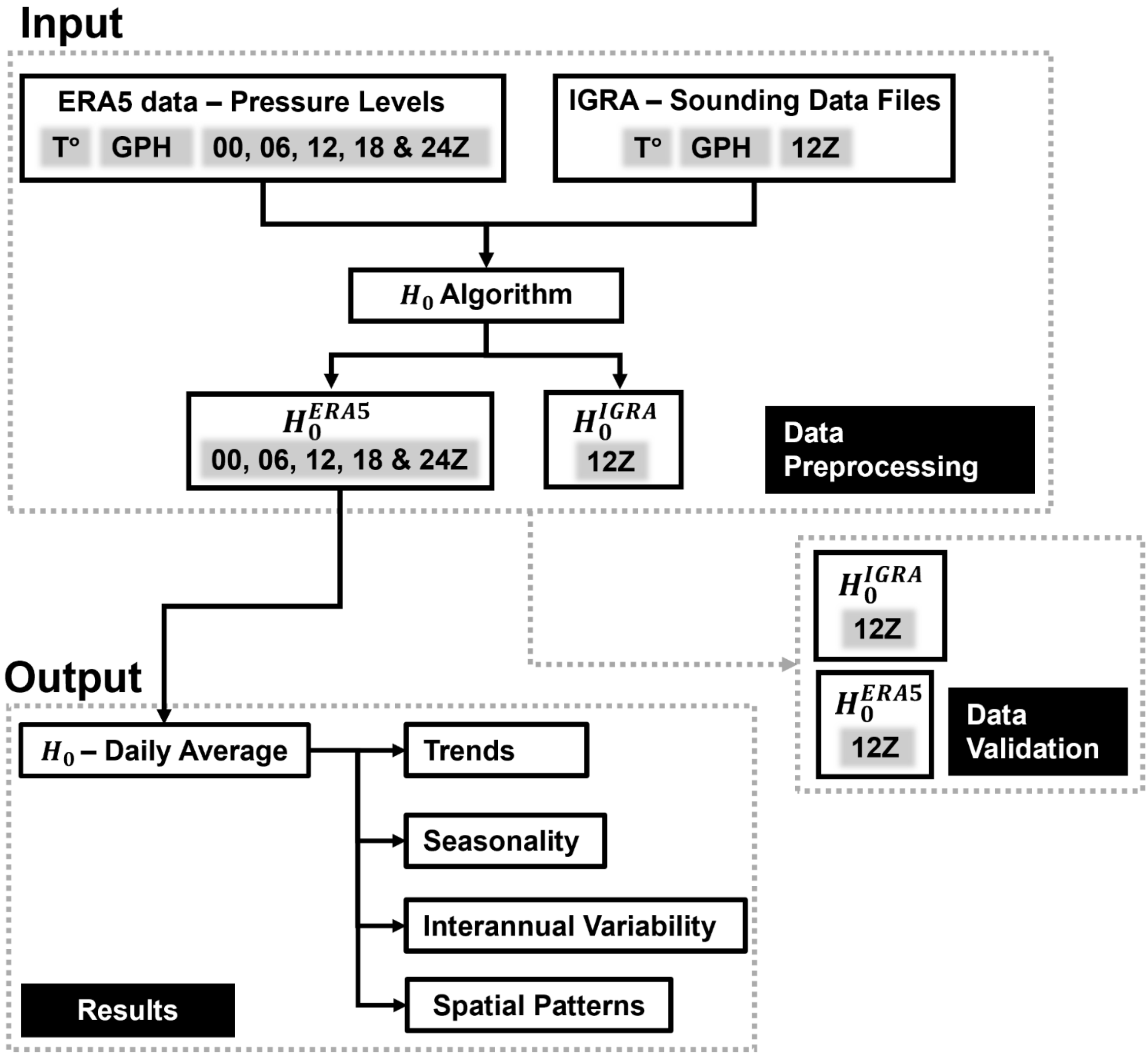

140 **Figure 2: The data processing workflow for H_0 between 1959 and 2021. Two distinct sets of input data were utilized: one comprising reanalysis data and the other containing radiosonde observations. The isotherm 0°C values were derived from these datasets, and a validation process was employed. Daily values were computed based on the reanalysis data.**

3 Results

3.1 Validation

The statistical analysis between pairs of time series is presented in Table 1 and Figure 3. The results unveil significant relationships among the variables under investigation. Notably, the freezing level in Puerto Montt, Comodoro Rivadavia, Río Gallegos and Punta Arenas demonstrates a consistently strong positive correlation throughout the entire period (r = 0.97, 0.96, 0.8, 0.94; respectively).

H_0^{ERA5} effectively captures the southern thermal gradient within the study area. This pattern becomes apparent when examining the decreasing average heights of H_0^{ERA5} from Puerto Montt (2278±980 m a.s.l) to Punta Arenas (1176±655 m a.s.l). The noticeable disparity between the averaged isotherms for the northern and southern points of the study area further reinforces this point.

Table 1. Data and statistics of validation process between daily values of H_0^{IGRA} and H_0^{ERA5}. First columns indicate latitude (Lat.), longitude (Lon.), period, and number of data available (n_{obs}). Others columns depicted statistics as Pearson correlation (r*, values that are statistically significant at a p-value < 0.05), mean values ($\bar{H}_0$), standard deviation (σ_0), mean bias error (MBE) and root mean-square error (RMSE).

	Lat.	Lon.	Period	n_{obs}	r*	$\bar{H}_0^{IGRA}$	$\bar{H}_0^{ERA5}$	MBE	σ_0^{IGRA}	σ_0^{ERA5}	RMSE
Puerto Montt	-41.435	-73.098	1959-2021	21251	0.97	2314	2278	-36	961	980	252
Comodoro Rivadavia	-45.783	-67.500	1959-2021	17157	0.96	2100	2069	-30	864	869	240
Río Gallegos	-51.633	-69.217	1967-1977	2194	0.8	1487	1380	-107	714	633	445
Punta Arenas	-53.003	-70.845	1975-2021	11494	0.94	1287	1176	-111	655	655	251

The mean bias error (MBE) between H_0^{ERA5} and H_0^{IGRA} values are negative at each comparison point, indicating an underestimation of the freezing level height by the ERA5 reanalysis. The smaller MBE were estimated in the northern zone, reaching an absolute minimum of 30 meters in Comodoro Rivadavia, followed by Puerto Montt with 36 meters. The larger biases were obtained for the southernmost zone, reaching an absolute maximum of 111 meters in Punta Arenas, closely followed by Río Gallegos at 107 meters. The calculated standard deviation for each pair of points was remarkably similar. The root mean square error for the longest series (Puerto Montt and Comodoro Rivadavia) ranges from 240-252 m a.s.l. For Río Gallegos, which has the smallest number of observations (barely a decade), the root mean square error increases to 445 m a.s.l. Despite this increase, the average value of the data is not exceeded in any case by the RMSE; which indicates, the uncertainty is contained in the means of the data. For more details and calculations using the observations, please refer to the supplementary material section. Additional results from the comparison of observed and reanalysis data are provided in the supplementary material (Table S1 and Table S2).

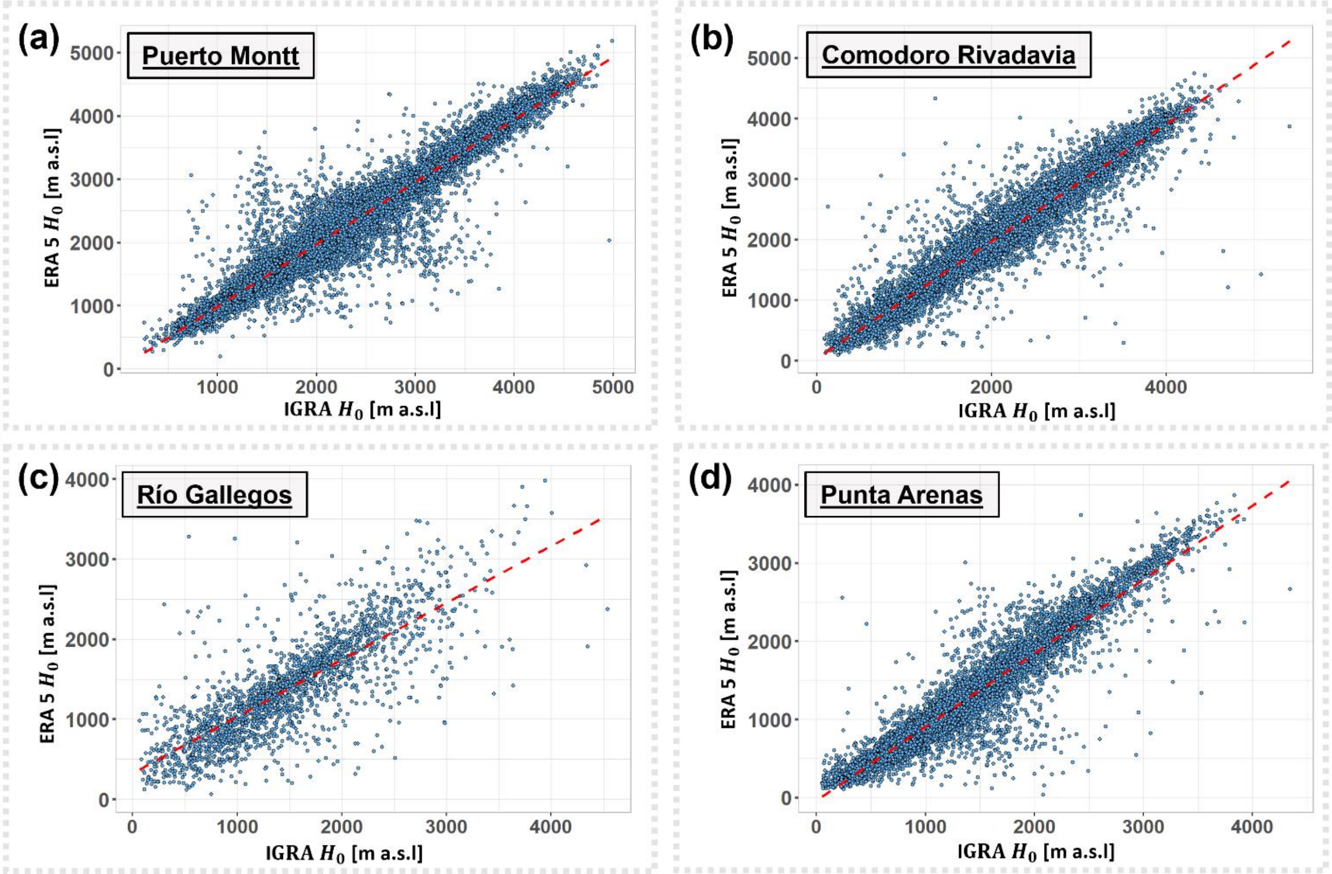

Figure 3: Scatterplots from Puerto Montt (a), Comodoro Rivadavia (b), Río Gallegos (c) and Punta Arenas (d). The reference data corresponds to H_0^{ERA5}(closest grid point) and **H_0^{IGRA}. The red dotted line in scatterplots shows the 1:1 line.**

3.2 Spatial patterns of H_0

The annual average of the H_0 field in the zone reveals a north-to-south variation, with higher height in the northern region and lower height in the southern region (Figure 4). The latitudinal profile (Figure 4b) shows a gradual decrease, intersecting with the topography between 47°-51°S. The interquartile range in the latitudinal profile (IQR_m) fluctuates from 905 to 2626 m a.s.l, and capture the extent of variations within the highest levels of the topography.

Conversely, the longitudinal profile (Figure 4c) exhibits an abrupt change in H_0 between 70°-74°W, coinciding with the presence of the highest peaks of the AA. The zone exhibits a broad range in the longitudinal interquartile range (IQR_z) ranging from 705 to 2654 m a.s.l, indicating significant variability in the H_0, which surpasses that of IQR_m. Besides, the IQR_z range encompasses the freezing level's proximity close to the lowest topography on the western side of the area. In the eastern region, the IQR_z range approaches H_0 only at the highest topography on the eastern side. Spatially, the region demarcated by higher isotherms forms a ridge, with its axis extending over the eastern side. In contrast, lower isotherms delineate a trough, with its axis extending over the western side. Notably, the difference between the western and eastern sides of H_0 occurs above the highest section of the AA, around 70° to 74°W (Figure 4c). To simplify and establish a clear transition zone between the western and eastern sides of H_0, we designate 72°W as the boundary longitude.

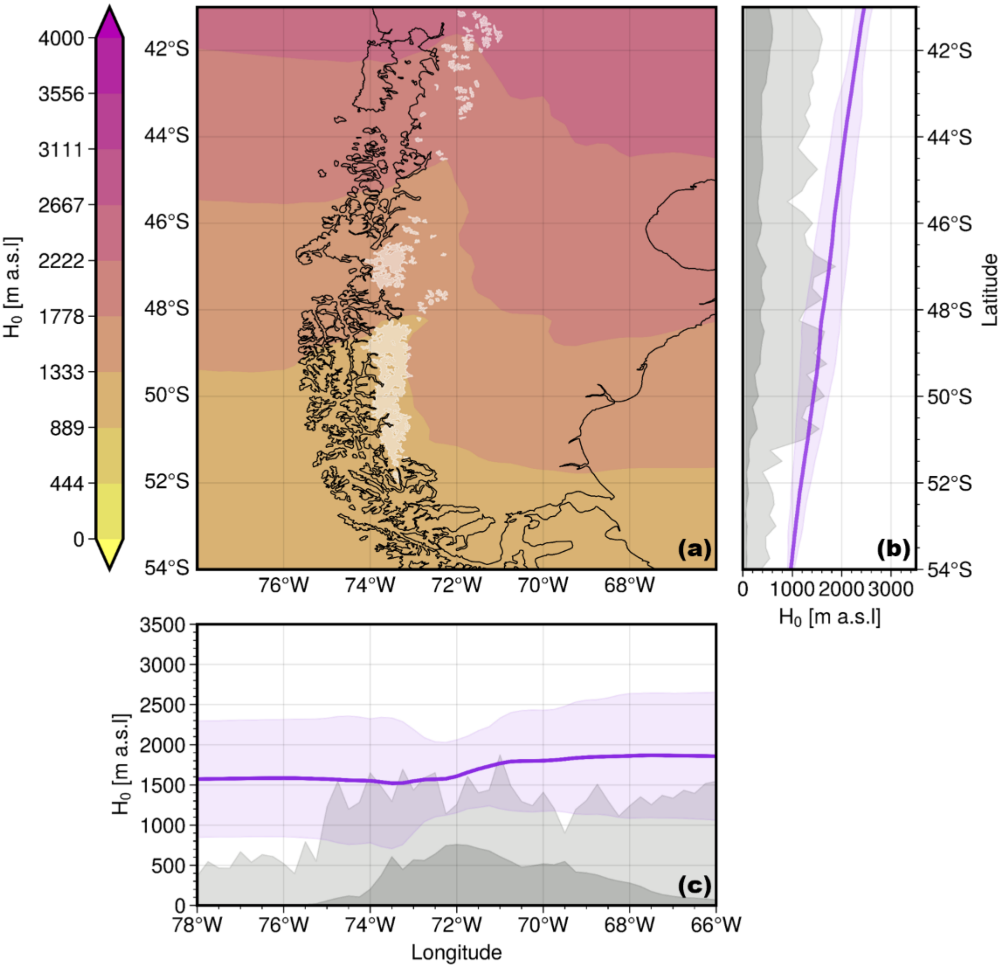

Figure 4: (a) Spatial distribution of the annual average of H_0. Lighter areas depict a lower height of H_0, while red areas indicate higher values. The white contours delineate the extent of ice coverage in the region. Each distribution is accompanied by a (b) latitudinal profile and (c) a longitudinal profile, showcasing the spatially averaged H_0 values. The purple shaded area in these profiles represents the respective interquartile range for each profile ($IQR_{m,z}$). The grey contours illustrate topographic profiles corresponding to the 2.5th percentile (dark grey) and 97.5th percentile (light grey).

Consequently, we used this meridian as a reference for a transitional boundary in the AA (Figure 4), demarcating a middle ground where various regional geographical features converge. In doing so, we define western Patagonia as the region situated west of the 72°W meridian, while eastern Patagonia lies east. Notable differences can be observed through a histogram displaying values from 1959 to 2021 for the entire region, as well as the western and eastern slopes of the AA (Figure 5). Firstly, the average and median values for the entire region are 1691 and 1519 m a.s.l, respectively (Table S3). Since the median is lower than the mean, the distribution exhibits positive skewness or is right-skewed. Notably, the upper extreme values (95th percentile) ascend to 3424 m a.s.l, while the lower extreme values (5th percentile) hover around 488 m a.s.l (Figure S1). Secondly, highlights the contrast in H_0 between western (blue line) and eastern (red line) Patagonia. Western Patagonia has a lower height, as indicated by a higher frequency of lower H_0 values with a mean and median which reach 1568 and 1347 m a.s.l, respectively. On the other hand, eastern Patagonia has higher frequency of, relatively, higher values, with a mean and median of 1818 and 1708 m a.s.l respectively. The two regions differ by approximately 251 (mean) to 362 m a.s.l (median) for the entire period. These values are shown in the supplementary material (Figure S1).

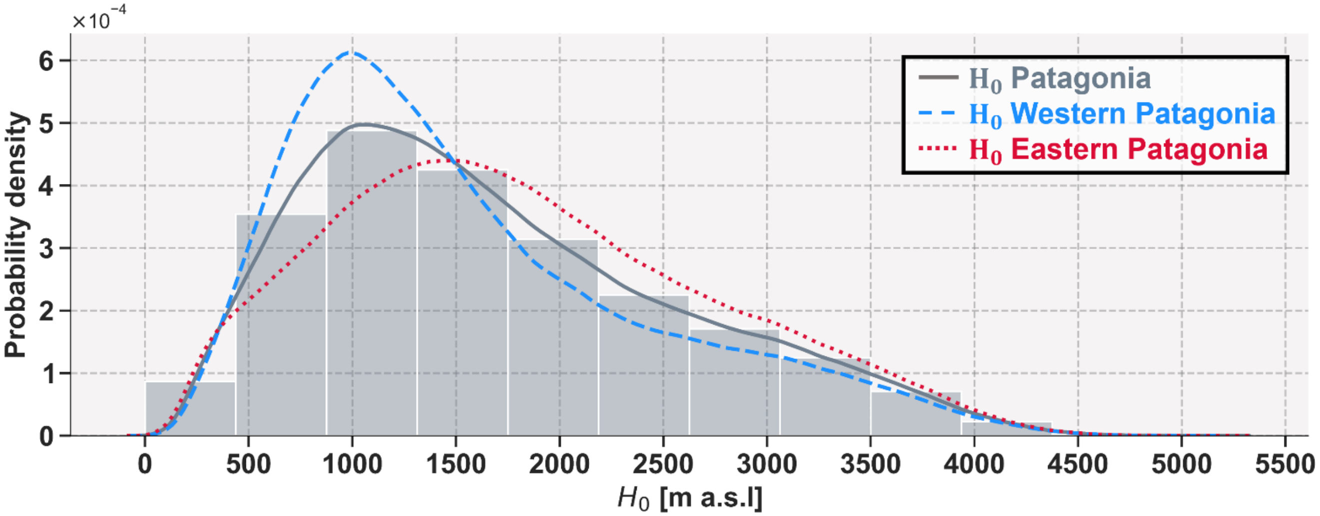

Figure 5: Histogram of daily simulated 0°C isotherm in Patagonia. The gray bars represent the daily values of H_0 obtained from the spatial average across the entire study area from 1959 to 2021. The curves, on the other hand, indicate the fit of the kernel density estimation for the entire region (gray), Western Patagonia (blue), and Eastern Patagonia (red).

3.3 Seasonal cycle of H_0

The average variations of H_0 from north to south exhibit a marked seasonality (Figure 6). During the summer months, a distribution with higher heights is observed, reaching peak values in the mid-summer (January-February) over the region. From March, there is a sustained decrease in H_0, reaching its lowest point during winter (July-August). The estimated mean amplitude indicates a range between 575 and 3346 m a.s.l (the highest absolute average in summer and winter). The average annual difference between the northernmost and southernmost zones of our study area is 1511 m a.s.l.

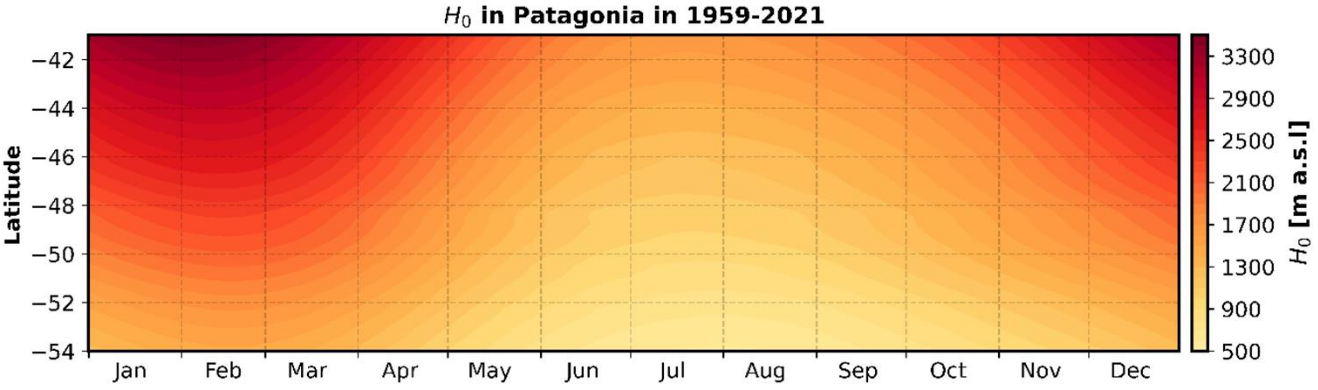

Figure 6: Latitudinal profile of daily climatology of H_0 in Patagonia from 1959 to 2021.

A detailed examination of the seasonal averages provides further insights into the characteristics of Patagonia's 0°C isotherm height (Figure 7). During summers, the average height of the isotherm is 2236 m a.s.l, while the spatial distribution indicates how the longitudinal bands change concerning the east-west side of the AA (72°W). The latitudinal profile of the isotherm and IQR indicates that during this season, the freezing level height varies from 3383 (northern area) to 1188 (southern area) m a.s.l. This implies that the lowest isotherms during this period slightly reach the highest summits of the topography around 49.5°-51°S. The longitudinal profile confirms that the longitudinal gradient intensifies around the AA, with values ranging from 3383 (eastern area) to 931 m a.s.l (western area) along the profile. Additionally, the lower range of the isotherm allows for interception with the high AA topography around 72.5-75°W.

In autumn, the decrease in the freezing level height is evident. During this season, the average isotherm drops to 1891 m a.s.l, while the variations in the latitudinal and longitudinal profiles are smaller than summer, ranging from 1066-2848 and 841-2858 m a.s.l, respectively.

During the winter months, the lowest values are recorded. In this season the mean value was estimated at 1169 m a.s.l, and the spatial variability range is narrower, spanning from 591-1799 (latitudinal range) and 447-1931 m a.s.l (longitudinal range). These conditions allow the 0°C isotherm to intercept a significant portion of the higher and even lower terrain, especially around 73.5°W, as indicated by the longitudinal profile.

At the spring, an average isotherm of 1477 m a.s.l was estimated, being the second lowest freezing level value after winter. For these months, an increase in the amplitude of the latitudinal and longitudinal isotherm ranges was already evident, with values ranging from 701-2449 and 596-2440 m a.s.l, respectively. However, despite the greater variability observed in the freezing level, the interception of the isotherm field with a significant portion of the higher terrain persists, particularly on the western slope of the Andes.

It is worth highlighting that the seasonal variations in Patagonia maintain and modulate the characteristic latitudinal and longitudinal gradient of the region, causing the estimated 0°C isotherm to fluctuate in a way that preserves its general spatial structure.

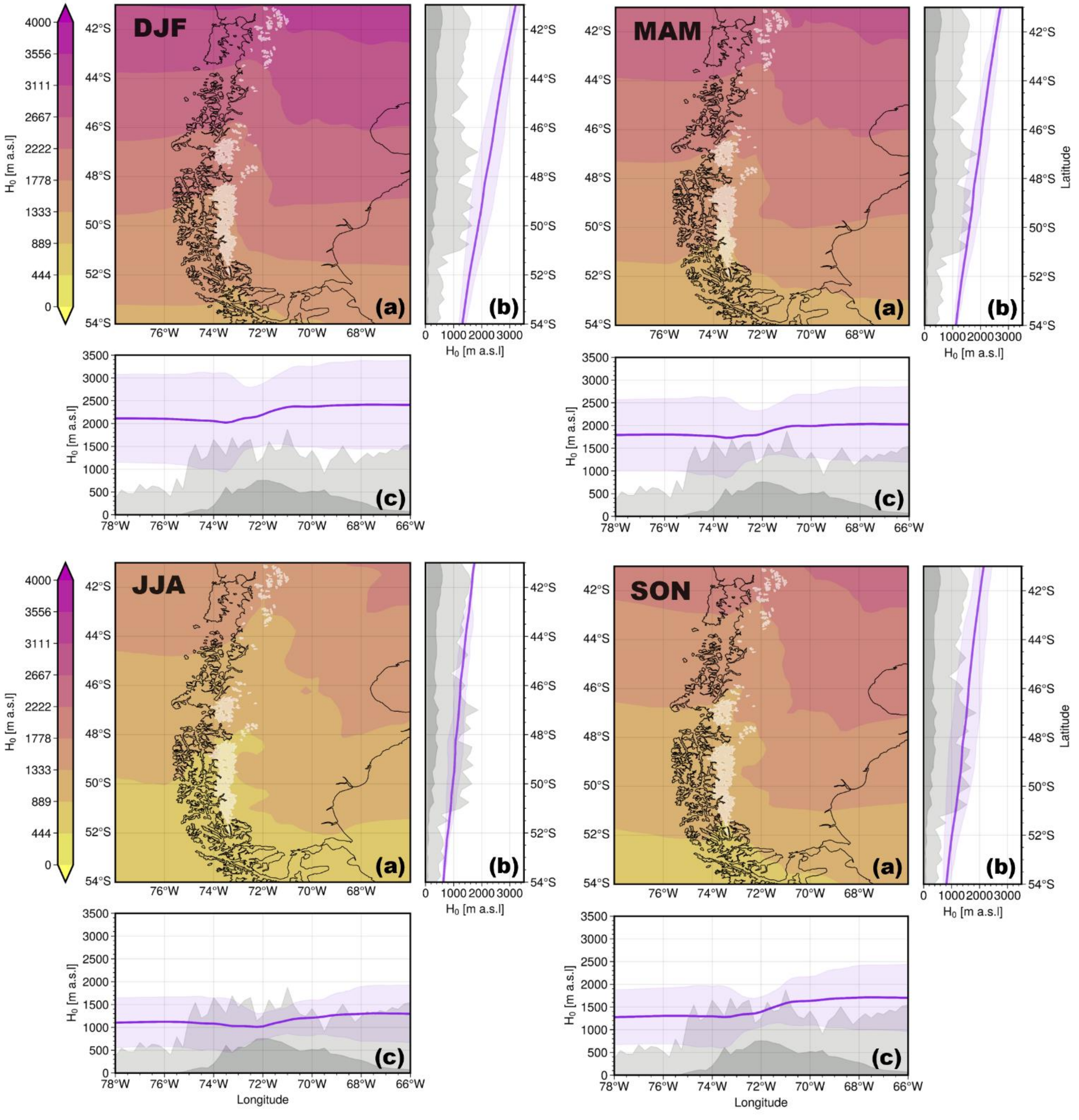

Figure 7: Spatial distribution of the seasonal averages of H_0 (a). Lighter areas depict a lower height of H_0, while red areas indicate higher values. The white contours delineate the extent of ice coverage in the region. Each seasonal distribution is accompanied by a latitudinal profile (b) and a longitudinal profile (c), showcasing the spatially averaged H_0 values. The purple shaded area in these profiles represents the respective interquartile range for each profile ($IQR_{m,z}$). The grey contours illustrate topographic profiles corresponding to the 2.5th percentile (dark grey) and 97.5th percentile (light grey).

3.4 Trends of H_0

From an annual perspective, our findings revealed positive and statistically significant trends in the freezing level across the region ($\bar{T}_0^{Annual} = 23.8$ m/decade, Table S5). Spatially, the highest average annual trend, reaching up to 36.5 m/decade, was observed in northwestern Patagonia, while the lowest, at 8.8 m/decade, was reported in the southernmost part of the region (Figure S2).

A seasonal analysis reveals that the summer season, has the most pronounced trends compared to other seasons ($\bar{T}_0^{DJF} = 40$ m/decade). This trend is particularly notable in the northwest region of Patagonia, reaching a maximum of 60.7 m/decade (Figure 8, DJF). The lowest values, reaching 18.1 m/decade.

The trends diminish during autumn ($\bar{T}_0^{MAM} = 36$ m/decade), and there is a shift in the spatial distribution of these trends (Figure 8, MAM). In contrast to the summers, the field becomes more homogeneous, with high trend values dispersed in the northwest and the central area, where a maximum of 45.5 m/decade is observed. Conversely, the minimum trend during this season is 17.5 m/decade.

In winters (Figure 8, JJA), the trend continues to decrease, reaching the second-lowest seasonal value ($\bar{T}_0^{JJA} = 19$ m/decade). The highest and lowest values during this season are 30.1 and 8.4 m/decade, respectively.

Spring shows the lowest trends ($\bar{T}_0^{SON} = 16$ m/decade). The spatial distribution of trend values is homogeneous; therefore, the latitudinal and longitudinal profiles are almost steady (Figure 8, SON). Considering the significant values, it is evident that this seasonal distribution is the most homogeneous, except for the northwestern and central Patagonia regions, where slight increases in the trend are observed, reaching a maximum value of 22.4 m/decade. The minimum estimated trend is located over Tierra del Fuego, with a value of 10.5 m/decade

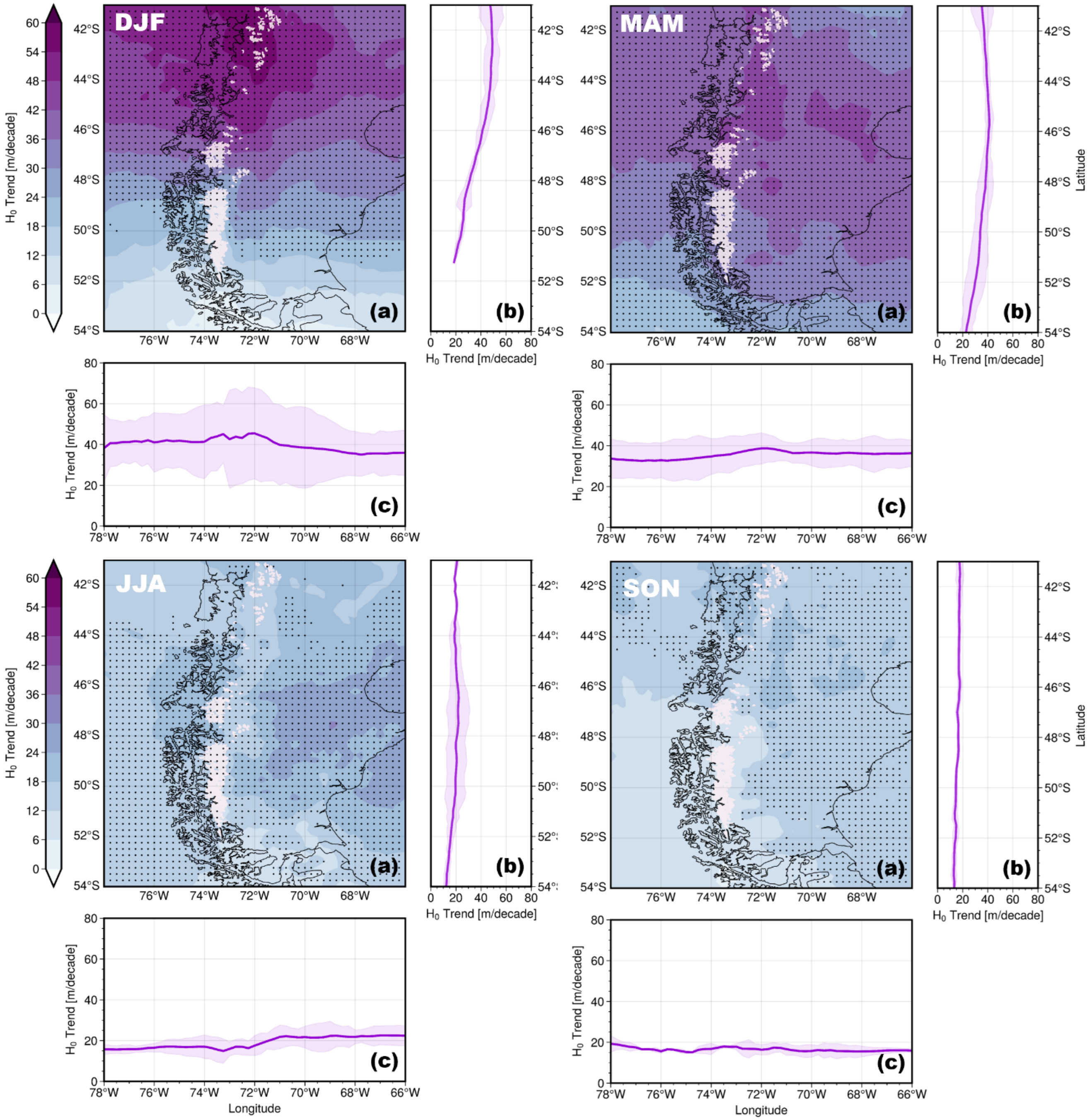

Figure 8: Spatial distribution of the 0°C isotherm trends (H_0) across the seasons. Lighter areas depict a lower height of the trends, while purple areas indicate higher values. The white contours delineate the extent of ice coverage in the region. Each distribution is accompanied by a latitudinal profile (b) and a longitudinal profile (c), showcasing the spatially averaged H_0 trend values. The purple shaded area in these profiles represents the respective interquartile range for each profile ($IQR_{m,z}$). Black circles denote statistically significant trends at p-value < 0.05.

3.5 Large-scale control over H_0 variability

To investigate the influence of other large-scale processes on the 0°C isotherm in Patagonia, we conducted an EOF analysis with annual anomalies of the 0°C isotherm (section 2.3). Following the methodology of North et al. (1982), we selected the first three principal modes (Figure S4), which together represent 96% of the interannual variability (Figure 9). The first mode of the EOF represents approximately 84% of the interannual variance of the 0°C isotherm in the region. Its spatial distribution represents a monopole that concentrates in the northwest region of Patagonia, coinciding with the spatial distribution of the trends recorded in the area (Figure 8a and Figure S2) and covering glacial areas and the northwest coast, approximately between 42-46°S. Figure 9b indicates the temporal component of the first mode, highlighting the high and significant correlation ($r=0.85$) between PC1 (red) and the average annual anomalies in the region (gray). In contrast, the second and third components show no significant relationship with H_0 anomalies ($|r| < 0.1$). Figure 9b also indicates that the 1970s and 2010s recorded the highest trends of annual anomalies of the 0°C isotherm (gray contours, 0.149 and 0.144 m/decade). According to our results, the most recent decade has presented the highest positive anomalies (Figure 9b), which coincide with a persistent positive phase of SAM since 2010 (Figure S4d; Fogt and Marshall, 2020). The correlations obtained between PC1 and SAM, R1-T850, and R2-SST (Figure 10) indicate significant and positive correlations ($r > 0.56$).

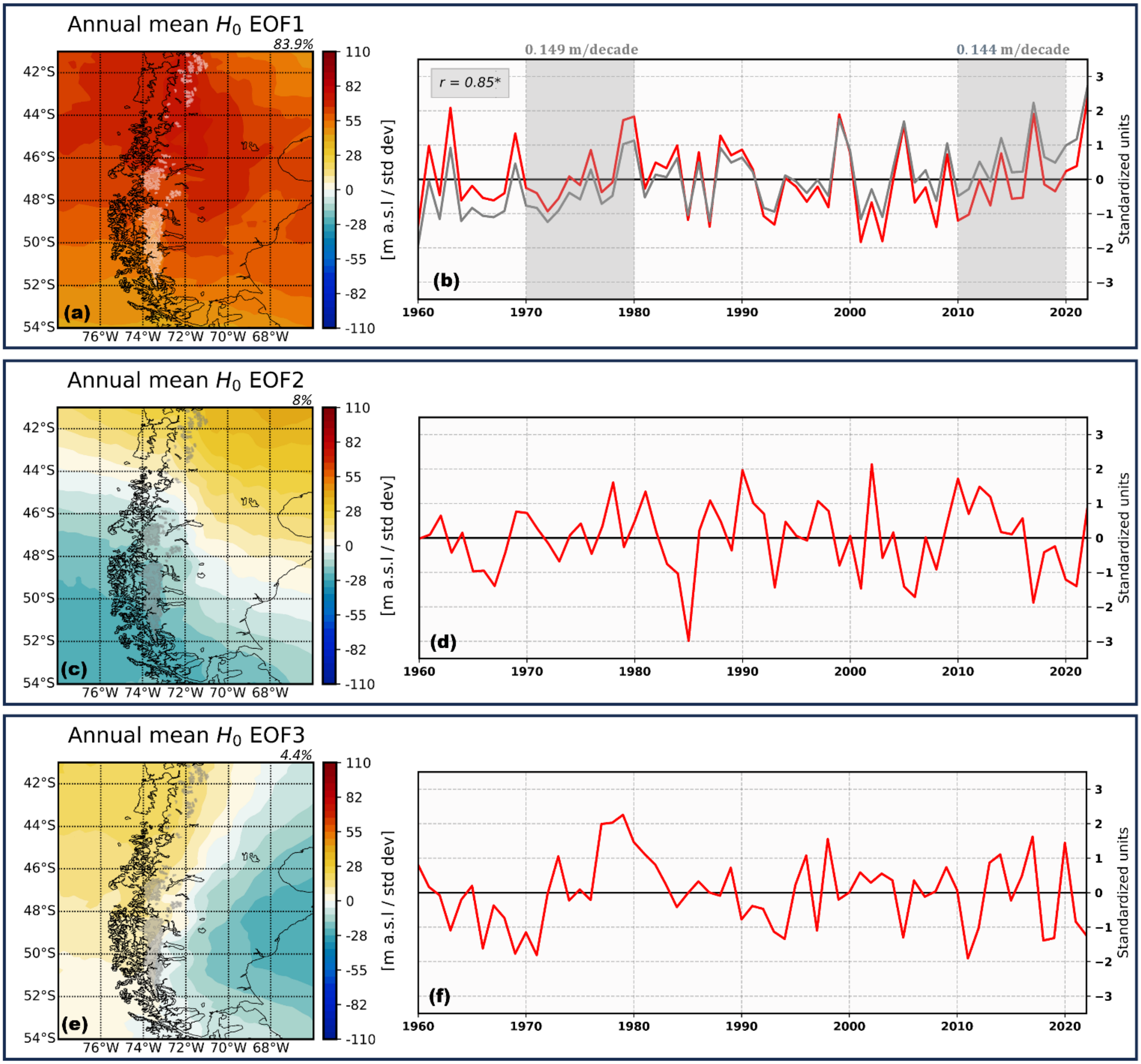

Figure 9: First three leading modes of variability extracted through an Empirical Orthogonal Function (EOF) analysis conducted on Patagonia's annual freezing level field spanning from 1959 to 2021. (a, c & e) The resulting patterns are presented as regression maps, illustrating the relationship between the leading Principal Component (PC) time series and the spatial distribution of the time-varying height anomalies. Additionally, the temporal pattern is illustrated by the first Principal Component (red line), scaled to unit variance (divided by the square root of its eigenvalue), while the grey line portrays the standardized anomalies of the spatial average of the annual freezing level field across Patagonia (b, d & f). In panel b, the grey box indicates Pearson's correlation between these two patterns and the grey contour area represents the periods with highest anomaly trend with their respective values. We continue the analysis for the second and third modes of variability (c-d and e-f, respectively). However, these modes show low correlation values with the freezing level anomalies, and thus, the focus is shifted away from freezing level anomalies in these cases. The white (a) and gray (c & e) contours delineate the extent of ice coverage in the region.

The second mode explains 8% of the variability of H_0 and is characterized by a latitudinal gradient, showing positive values in the northeast region and negative values in the southwest. The significant correlations are with the indices Z300 Drake ($r = -0.68$), T850 Drake ($r = -0.51$) and R3-U850 ($r = 0.53$). On the other hand, the third mode represents around 4% of the variability of H_0. It displays a longitudinal gradient with positive values in the northwestern side and negative values in the southeast. Significant correlation between pairs of indices and this mode only was found with Z300 Drake ($r = 0.39$) and R3-U850 ($r = -0.41$). Additionally, the correlation obtained from indices such as ENSO (NIÑO 1+2 and NIÑO 3.4) with the leading modes showed low and non-statistically significant correlations ($|r|<0.2$).

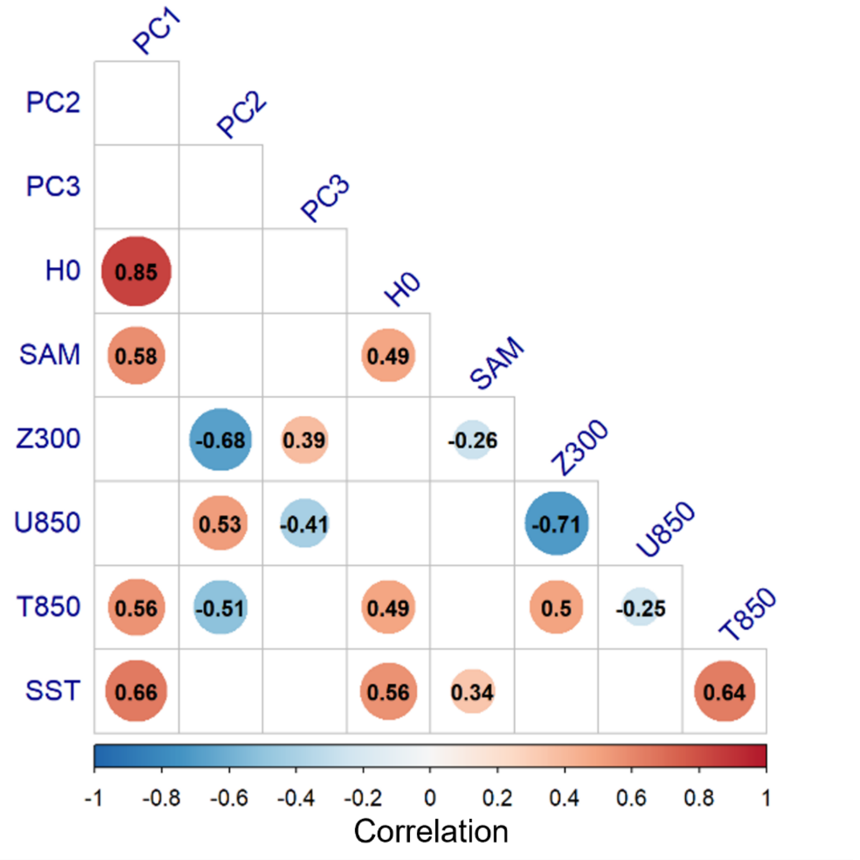

Figure 10: Correlation matrix between the standardized indices, H_0 anomalies, and principal components obtained from the analysis. Only statistically significant values (p-value < 0.05) are shown.

4 Discussion

1. The 0°C isotherm and ERA5 reanalysis.

The validation process indicated a high similarity between the 0°C isotherm values obtained from radiosondes and the reanalysis data. The greatest uncertainty occurred in Río Gallegos; however, the validation parameters (i.e. correlation, bias, standard deviation, and RMSE) are acceptable. This is especially noteworthy considering that radiosonde data in Río Gallegos compass a shorter period (n=2194, 1967-1977) compared to other launch sites, representing approximately 10% of the data compared to Puerto Montt, which has the highest number of records (n=21251).

However, we observed an underestimation of the 0°C isotherm calculated from reanalysis data when compared with 0° isotherm derived from radiosonde stations. Overall underestimation of the 0°C isotherm obtained from the ERA5 reanalysis has been documented previously by Schauwecker et al. (2022). They estimated an underestimation (overestimation) at low (high) elevation sites by the reanalysis, but reasons were not discussed. In our case, all radiosonde points are located near sea level with heights not exceeding 84 m above sea level, therefore the underestimation is consistent with findings by Schauwecker et al. (2022). To explore this feature, we conducted seasonal validation and comparison (Table S2). During the summer (December to February), the underestimation of the reanalysis was lower compared to winter (June-August) at stations on the west side (Puerto Montt and Punta Arenas). Conversely, at stations on the east side (Comodoro Rivadavia and Río Gallegos), the underestimation decreased (increased) during winter (summer) months. In our study area, we hypothesized that the underestimation of the reanalysis data may be linked to the environmental conditions of the radiosonde launch location points. For instance, topographic conditions are similar (i.e. low elevation, nearby to the sea, and more than 30 km away from larger topographic barrier such as the AA). However, further research and more data (stations or radiosondes) are necessary to better understand the underestimation of the reanalysis and its regional differences in Patagonia.

2. The 0°C isotherm in Patagonia.

It is well documented that the orographic influence of the Andes in Patagonia generates meteorological gradients (e.g., precipitation, temperatures, cloudiness, radiation) between the western and eastern sectors, (i.e. Garreaud et al., 2009; Garreaud et al., 2013). The 0°C isotherm is not the exception, showing clear longitudinal differences, with warmer conditions in the eastern sector compared to the western sector. This has implications in the type of precipitation (liquid or solid) and its spatial difference for a given same latitude, as has been reported previously (i.e. Viale et al., 2019). However, our results indicate that, south of 52°S, the difference between the western and eastern zones decreases, due to the topographic descent of the AA. This is consistent with the analysis of the annual cycle indicated by Garreaud et al. (2009), which shows that temperature differences between both sectors decrease at this latitude (see Figure S5).

Finally, it is worth noting that our trend results are comparable with other values reported in the area by Aguayo et al. (2019), who estimated a seasonal trend (DJF, 1970-2018) of 50 m/decade in the Puelo River basin (Figure 8a and Table S1).

3. Large-scale drivers.

Similar to the analysis conducted with the SAM (Figure 10 and Figure S6), a spatial and temporal correlation analysis was also performed to investigate possible links with other large-scale indices such as ENSO (1+2 and 3.4) and PDO (analysis not shown). However, no significant correlations were found to suggest any relationship between these indices and the 0°C isotherm in the region. On the other hand, the strong correlation between PC1 and annual anomalies of the 0°C isotherm, SAM, R1-T850, and R2-SST could provide clues to an interaction mechanism involving all variables. It has been documented by Garreaud et al., (2009), that during the positive phase of SAM, adiabatic warming occurs due to subsidence at the north of the polar jet, resulting in drier conditions in northern Patagonia; while southern Patagonia would experience wetter than normal conditions. Opposite conditions occur during the negative phase of SAM. The relationship between the positive phase of SAM and the warming of sea surface temperature in the western Pacific has also been documented (Thomas et al., 2017). Given the high correlation between SAM and SST, it is unknown whether it is possible to explain a mechanism that decouples processes between these variables to better understand their involvement in 0°C isotherm variations. However, the positive feedback mechanism between SAM (higher temperatures in northern Patagonia) and SST (increased Pacific temperature) could be contributing to the increase in the 0°C isotherm in northwest Patagonia. Our results are consistent with projections in the area, which point to drier conditions for northwest Patagonia under high greenhouse gas emissions scenarios by the end of the century (Collins et al., 2013). Regarding the southern zone and EOF1, the highest spatial correlations obtained involve sea surface temperature (R2-SST) and temperature over the Drake Passage (R1-T850), particularly in the southwest zone.

Given the correlations of the second principal component (Figure 10), we believe this mode may be related to clear sky conditions that favour a near-surface inversion layer. For example, before events with positive values of R1-Z300 and R1-T850 (conditions of a ridge passage over the Drake Passage), the values of H_0 will decrease (lower freezing level). In terms of PC2 and R3-U850 (r=0.53), the zonal wind could contribute to this process; westward zonal winds (u>0) force the passage of these systems. According to the spatial configuration of this mode, the described mechanism would be limited to the southwest zone of the region.

Finally, the third mode (EOF3) presents significant and positive correlations with R1-Z300 and negative correlations with R3-U850. We associated these correlations with the passage of a migratory high in the region, which generates favourable conditions for the generation of Puelche winds characterised by negative zonal winds (u<-4 m/s), descending and compressing adiabatically leeward, injecting high temperatures into the western zone of the AA, especially the southwest zone. Indeed, this synoptic configuration is associated with the increase of heatwaves events in the area since 1980 (Gonzalez-Reyes et al., 2023). Additionally, Figure 9b indicates the temporal variation of the principal component along with the 0°C isotherm anomalies. In the last decade, a period of persistent positive anomalies and an increasing trend of the 0°C isotherm (0.144 m/decade) can be observed. Further a decrease in precipitation in northwest Patagonia between 2010-16 has been reported, with an extreme drought period during the summer of 2016 (Garreaud et al., 2018). This period coincides with a positive trend of the 0°C isotherm in the last decade, making it an area of special attention and monitoring.

4. Impact on Patagonian Glaciers

Patagonia is characterized by extensive ice fields as Southern Patagonia Icefield, Northern Patagonia Icefield and Cordillera Darwin. As exposed by Caro et al. (2021), glacier surface mass balance depends on many factors such as precipitation, temperature, slope, orientation, and others. Because of this, quantifying glacier variations in a region where the 0°C isotherm is rising is complex. Estimated rise in the 0°C isotherm impact the surface mass balance, especially those situated in the northwest region. The consequences of freezing level rise will vary depending on the sensitivity of each glacier's mass balance and its specific topographic characteristics, such as the area of accumulation versus the area of ablation of a specific glacier. Sensitivity analysis by Caro et al. (2021), determined that glaciers are primarily sensitive to temperature changes in Patagonia. However, if we also consider a future scenario with higher concentration of greenhouse gases and radiative forcing (i.e. under SSP5-8.5 scenario), we hypothesize a rise in the height of the 0°C isotherm, leading to a decrease in solid precipitation in the area. This would affect water resources due to the reduction of glacier volumes (lower accumulation) and increase the region's vulnerability to natural hazards such as floods and Glacier Lake Outburst Floods (GLOFs) (Dussaillant et al., 2010; Piret et al., 2022).

5 Conclusions

Through vertical temperature profiles, values of the 0°C isotherm height were obtained using radiosonde observations and ERA5 data from 1959-2021 in Patagonia. The reanalysis data showed robust estimation of daily observed values and facilitated the derivation of spatial averages that describe the state of the 0°C isotherm within the study area. The relationship between the main atmospheric modes of 0°C isotherm interannual variability and time series of different climatic indices was investigated employing correlations. This approach aimed to discern the large-scale climatic processes governing interannual variations of the freezing level in Patagonia. Some significant findings are:

The histogram of spatial averages indicates a right-skewed distribution in H_0 Patagonia. Specifically, in the western Andes zone (western section of 72°W), the annual average (median) altitude is approximately 1568 (1347) m a.s.l. In contrast, the eastern Andes zone exhibits a mean (median) of 1818 (1709) m a.s.l. The annual values of the 0°C isotherm in Patagonia ranging from 2658 m a.s.l in the north to 913 m a.s.l in the south. The spatio-temporal annual average (median) of the field is 1691 (1519) m a.s.l.

Seasonal variations indicate that the 0°C isotherm's amplitude spans from 3346 (summer) to 575 m a.s.l (winter).

A pronounced longitudinal gradient is noteworthy, intensifying around 72°W, associated with a drier atmosphere influenced by the orographic lee-side effect of the Andes. The latitudinal gradient behaves as expected (typical temperature gradient of the transition to extratropic), gradually decreasing southward with latitude. This spatial configuration persists throughout the months, with the distinction that higher freezing level heights are recorded during summers. In this season, the longitudinal average is estimated not to intersect with the highest topography (95th percentile of topography). Contrasting conditions prevail during winter, where the lowest freezing level values are observed, and on average, the longitudinal profile of the 0°C isotherm intersects the highest (P95) and lowest (P5) topography around 72°W, essentially aligning with the Andes Mountain range. Autumn and spring months are transitional periods between the more pronounced summer and winter seasons.

Throughout the years, the 0°C isotherm level in Patagonia exhibited a consistent variation with temperature changes, marked by an increase in temperature within the whole region. This temperature shift translates into an annual spatial average increase in the freezing level height, ranging from 36.5 to 8.8 m/decade. Seasonally, the highest trends were observed during summers, specifically in northwestern Patagonia, around the Andes, indicating an average increase in freezing heights of 61 m/decade. On average, winter trends are lower but remain positive, reaching average values of 8.4 m/decade in areas surrounding the Andes.

The primary mode of variability accounts for about 84% of the variance in the H_0 field. Spatially, this mode shows predominantly positive values across the entire area, notably in central and northeastern Patagonia, which aligns with the locations of the highest estimated trends. Temporally, this mode shares interannual variability with Patagonia's average field of 0°C isotherm anomalies. Thus, years with positive phases of the first principal component (PC1) are associated with positive anomalies in freezing level height. Similarly, this mode shows a positive and significant correlation with SAM, temperature at 850 hPa in the Drake Passage, and sea surface temperature in the Pacific Ocean near the western coasts of Patagonia. The second and third modes explain 8% and 4.4% of the data variance, respectively. Their spatial configuration indicates both a latitudinal and longitudinal dipole in the study area. The second mode exhibited significant correlations with R1-Z300 (+), R1-T850 (-), and R3-U850 (-). Meanwhile, the third mode significantly correlated with R1-300 (+) and R3-U850 (-).

Code availability

Preprocessing script along with the corresponding files are available at https://doi.org/10.5281/zenodo.10523940 (García-Lee and Mardones, 2024).

Data availability

ERA5 pressure levels (Hersbach et al., 2023) was acquired from the Copernicus climate data store.

Author contributions

All authors participated in the conceptualization and methodology of the research. CB and AGR proposed the research topic. NG and PM carried out the software development, data curation and analysis. NG was in charge of project administration, resources, validation, visualization and draft writing. All authors contributed to the review and editing of the manuscript.

Acknowledgments

We thank Dr. Simone Schauwecker for her assistance during the manuscript draft review phase. We acknowledge the contribution of the AI translator tool in the English writing process, enabling us to enhance the communication of ideas within the manuscript.

References

Abram, N. J., Mulvaney, R., Vimeux, F., Phipps, S. J., Turner, J., & England, M. H. Evolution of the Southern Annular Mode during the past millennium. Nature Climate Change, 4(7), 564-569. https://doi.org/10.1038/nclimate2235, 2014.

Aravena, J. C., & Luckman, B. H. Spatio-temporal rainfall patterns in Southern South America. International Journal of Climatology, 29(14), 2106–2120. https://doi.org/10.1002/JOC.1761, 2009.

Aguayo, R., León-Muñoz, J., Vargas-Baecheler, J., Montecinos, A., Garreaud, R., Urbina, M., ... & Iriarte, J. L. The glass half-empty: climate change drives lower freshwater input in the coastal system of the Chilean Northern Patagonia. *Climatic Change*, *155*, 417-435. https://doi.org/10.1007/s10584-019-02495-6, 2019.

Crameri, F. Scientific colour maps. *Zenodo*, *10*. 10.5281/zenodo.1243862, 2018.

Bravo, C., Bozkurt, D., Gonzalez-Reyes, Á., Quincey, D. J., Ross, A. N., Farías-Barahona, D., & Rojas, M. Assessing snow accumulation patterns and changes on the Patagonian Icefields. Frontiers in Environmental Science, 30. https://doi.org/10.3389/fenvs.2019.00030, 2019.

Bravo, C., Ross, A. N., Quincey, D. J., Cisternas, S., & Rivera, A. Surface ablation and its drivers along a west–east transect of the Southern Patagonia Icefield. Journal of Glaciology, 68(268), 305-318. https://doi.org/10.1017/jog.2021.92, 2022.

Carrasco, J. F., Casassa, G., & Rivera, A. Meteorological and climatological aspects of the Southern Patagonia Icefield. In The Patagonian Icefields: A unique natural laboratory for environmental and climate change studies (pp. 29-41). Boston, MA: Springer US. https://doi.org/10.1007/978-1-4615-0645-4_4, 2002.

Carrasco-Escaff, T., Rojas, M., Garreaud, R. D., Bozkurt, D., & Schaefer, M. Climatic control of the surface mass balance of the Patagonian Icefields. The Cryosphere, 17(3), 1127-1149. https://doi.org/10.5194/tc-17-1127-2023, 2023.

Durre, I., Yin, X., Vose, R. S., Applequist, S., & Arnfield, J. Enhancing the data coverage in the Integrated Global Radiosonde Archive. Journal of Atmospheric and Oceanic Technology, 35(9), 1753-1770. https://doi.org/10.1175/JTECH-D-17-0223.1, 2018.

Caro, A., Condom, T., & Rabatel, A. Climatic and morphometric explanatory variables of glacier changes in the Andes (8–55 S): New insights from machine learning approaches. Frontiers in Earth Science, 9, 713011. https://doi.org/10.3389/feart.2021.713011, 2021.

Collins, M., R. Knutti, J. Arblaster, J.-L. Dufresne, T. Fichefet, P. Friedlingstein, X. Gao, W.J. Gutowski, T. Johns, G. Krinner, M. Shongwe, C. Tebaldi, A.J. Weaver, and M. Wehner. Long-term climate change: Projections, commitments and irreversibility. In Climate Change 2013: The Physical Science Basis. Contribution of Working Group I to the Fifth Assessment Report of the Intergovernmental Panel on Climate Change. T.F. Stocker, D. Qin, G.-K. Plattner, M. Tignor, S.K. Allen, J. Doschung, A. Nauels, Y. Xia, V. Bex, and P.M. Midgley, Eds., Cambridge University Press, pp. 1029-1136, doi:10.1017/CBO9781107415324.024, 2013.

Dussaillant J, A., Buytaert, W., Meier, C., & Espinoza, F. Hydrological regime of remote catchments with extreme gradients under accelerated change: the Baker basin in Patagonia. Hydrological sciences journal, 57(8), 1530-1542. https://doi.org/10.1080/02626667.2012.726993, 2012.

Dussaillant, A., Benito, G., Buytaert, W. et al. Repeated glacial-lake outburst floods in Patagonia: an increasing hazard?. Nat Hazards 54, 469–481. https://doi.org/10.1007/s11069-009-9479-8, 2010.

Fogt, R. L., & Marshall, G. J. The Southern Annular Mode: variability, trends, and climate impacts across the Southern Hemisphere. Wiley Interdisciplinary Reviews: Climate Change, 11(4), e652. https://doi.org/10.1002/wcc.652, 2020.

Nicolás D. García-Lee, N., & Piero Mardones. Spatial and temporal variability of freezing level in Patagonia's atmosphere [Data set]. En Weather and Climate Dynamics. Zenodo. https://doi.org/10.5281/zenodo.10523940, 2024.

Garreaud, R. D., Vuille, M., Compagnucci, R., & Marengo, J. Present-day south american climate. Palaeogeography, Palaeoclimatology, Palaeoecology, 281(3-4), 180-195. https://doi.org/10.1016/j.palaeo.2007.10.032, 2009.

Garreaud, R., Lopez, P., Minvielle, M., & Rojas, M. Large-scale control on the Patagonian climate. Journal of Climate, 26(1), 215-230. https://doi.org/10.1175/JCLI-D-12-00001.1, 2013.

Garreaud, R. D. Record-breaking climate anomalies lead to severe drought and environmental disruption in western Patagonia in 2016. Climate Research, 74(3), 217-229. https://doi.org/10.3354/cr01505, 2018.

Hao, X., He, S., Wang, H. *et al*. The impact of long-term oceanic warming on the Antarctic Oscillation in austral winter. *Sci Rep* **7**, 12321. https://doi.org/10.1038/s41598-017-12517-x. 2017.

González-Reyes, Á., Jacques-Coper, M., Bravo, C., Rojas, M., & Garreaud, R. Evolution of heatwaves in Chile since 1980. Weather and Climate Extremes, 41, 100588. https://doi.org/10.1016/j.wace.2023.100588, 2023.

Hersbach, H., Bell, B., Berrisford, P., Hirahara, S., Horányi, A., Muñoz-Sabater, J., Nicolas, J., Peubey, C., Radu, R., Schepers, D., Simmons, A., Soci, C., Abdalla, S., Abellan, X., Balsamo, G., Bechtold, P., Biavati, G., Bidlot, J., Bonavita, M., ... Thépaut, J. N. The ERA5 global reanalysis. Quarterly Journal of the Royal Meteorological Society, 146(730), 1999-2049. https://doi.org/10.1002/qj.3803, 2020.

Hugonnet, R., McNabb, R., Berthier, E., Menounos, B., Nuth, C., Girod, L., Farinotti, D., Huss, M., Dussaillant, I., Brun, F., & Kääb, A. Accelerated global glacier mass loss in the early twenty-first century. Nature, 592(7856), 726-731. https://doi.org/10.1038/s41586-021-03436-z, 2021.

Hussain, M., Mahmud, I. pyMannKendall: a python package for non parametric Mann Kendall family of trend tests. Journal of Open Source Software, 4(39), 1556, https://doi.org/10.21105/joss.01556, 2019.

Iribarren-Anacona, P., Mackintosh, A., & Norton, K. P. Hazardous processes and events from glacier and permafrost areas: lessons from the Chilean and Argentinean Andes. Earth Surface Processes and Landforms, 40(1), 2-21. https://doi.org/10.1002/ESP.3524, 2015.

King, J., Anchukaitis, K. J., Allen, K., Vance, T., & Hessl, A. Trends and variability in the Southern Annular Mode over the Common Era. Nature Communications, 14(1), 2324. 10.1038/s41467-023-37643-1, 2023.

Lenaerts, J. T., van den Broeke, M. R., van Wessem, J. M., van de Berg, W. J., van Meijgaard, E., van Ulft, L. H., & Schaefer, M. Extreme precipitation and climate gradients in Patagonia revealed by high-resolution regional atmospheric climate modeling. Journal of climate, 27(12), 4607-4621. https://doi.org/10.1175/JCLI-D-13-00579.1, 2014.

Malz, P., Meier, W., Casassa, G., Jaña, R., Skvarca, P., & Braun, M. H. Elevation and mass changes of the Southern Patagonia Icefield derived from TanDEM-X and SRTM data. Remote Sensing, 10(2), 188. https://doi.org/10.3390/rs10020188, 2018.

Mardones, P., & Garreaud, R. D. Future changes in the free tropospheric freezing level and rain–snow limit: The case of central Chile. Atmosphere, 11(11), 1259. https://doi.org/10.3390/atmos11111259, 2020.

Marshall, G. J. Trends in the Southern Annular Mode from observations and reanalyses. Journal of climate, 16(24), 4134-4143. https://doi.org/10.1175/1520-0442(2003)016<4134:TITSAM>2.0.CO;2, 2003.

Masiokas, M. H., Rabatel, A., Rivera, A., Ruiz, L., Pitte, P., Ceballos, J. L., ... & MacDonell, S. A review of the current state and recent changes of the Andean cryosphere. Frontiers in Earth Science, 8, 99. https://doi.org/10.3389/feart.2020.00099, 2020.

Minowa, M., Schaefer, M., Sugiyama, S., Sakakibara, D., & Skvarca, P. Frontal ablation and mass loss of the Patagonian icefields. Earth and Planetary Science Letters, 561, 116811. https://doi.org/10.1016/j.epsl.2021.116811, 2021.

Morgenstern, O. The southern annular mode in 6th coupled model intercomparison project models. *Journal of Geophysical Research: Atmospheres*, *126*(5), e2020JD034161. https://doi.org/10.1029/2020JD034161, 2021.

Montecinos, A., Muñoz, R. C., Oviedo, S., Martínez, A., & Villagrán, V. Climatological characterization of puelche winds down the western slope of the extratropical Andes Mountains using the NCEP Climate Forecast System Reanalysis. Journal of Applied Meteorology and Climatology, 56(3), 677-696. https://doi.org/10.1175/JAMC-D-16-0289.1, 2017.North, G. R., Bell, T. L., Cahalan, R. F., & Moeng, F. J. Sampling errors in the estimation of empirical orthogonal functions. Monthly weather review, 110(7), 699-706. https://doi.org/10.1175/1520-0493(1982)110<0699:SEITEO>2.0.CO;2, 1982.

Piret, L., Bertrand, S., Nguyen, N., Hawkings, J., Rodrigo, C., & Wadham, J. Long-lasting impacts of a 20th century glacial lake outburst flood on a Patagonian fjord-river system (Pascua River). Geomorphology, 399, 108080. https://doi.org/10.1016/j.geomorph.2021.108080, 2022.

Roe, G. H. Orographic precipitation. Annu. Rev. Earth Planet. Sci., 33, 645-671. https://doi.org/10.1146/ANNUREV.EARTH.33.092203.122541, 2005.

Saavedra, F., Cortés, G., Viale, M., Margulis, S., & McPhee, J. Atmospheric rivers contribution to the snow accumulation over the southern Andes (26.5 S–37.5 S). Frontiers in Earth Science, 8, 261. https://doi.org/10.3389/feart.2020.00261, 2020.

Sauter, T. Revisiting extreme precipitation amounts over southern South America and implications for the Patagonian Icefields. Hydrology and Earth System Sciences, 24(4), 2003-2016. https://doi.org/10.5194/HESS-24-2003-2020, 2020.

Schauwecker, S., Rohrer, M., Huggel, C., Endries, J., Montoya, N., Neukom, R., Perry, B., Salzmann, N., Schwarb, M., & Suarez, W. The freezing level in the tropical Andes, Peru: An indicator for present and future glacier extents. Journal of Geophysical Research: Atmospheres, 122(10), 5172-5189. https://doi.org/10.1002/2016JD025943, 2017.

Shi, N., Tian, P., & Zhang, L. Simultaneous influence of the Southern Hemisphere annular mode on the atmospheric circulation of the Northern Hemisphere during the boreal winter. International Journal of Climatology, 39(5), 2685-2696. https://doi.org/10.1002/joc.5981, 2019.

Siler, N., Roe, G., & Durran, D. On the dynamical causes of variability in the rain-shadow effect: A case study of the Washington Cascades. Journal of Hydrometeorology, 14(1), 122-139. https://doi.org/10.1175/JHM-D-12-045.1, 2013.

Somos-Valenzuela, M. A., Oyarzún-Ulloa, J. E., Fustos-Toribio, I. J., Garrido-Urzua, N., & Chen, N. The mudflow disaster at Villa Santa Lucía in Chilean Patagonia: understandings and insights derived from numerical simulation and postevent field surveys. Natural Hazards and Earth System Sciences, 20(8), 2319-2333. https://doi.org/10.5194/NHESS-20-2319-2020, 2020.

Van Der Geest, K., & Van Den Berg, R. Slow-onset events: a review of the evidence from the IPCC Special Reports on Land, Oceans and Cryosphere. Current Opinion in Environmental Sustainability, 50, 109-120. https://doi.org/10.1016/J.COSUST.2021.03.008, 2021.

Thomas, E. R., van Wessem, J. M., Roberts, J., Isaksson, E., Schlosser, E., Fudge, T. J., Vallelonga, P., Medley, B., Lenaerts, J., Bertler, N., van den Broeke, M. R., Dixon, D. A., Frezzotti, M., Stenni, B., Curran, M., and Ekaykin, A. A.: Regional Antarctic snow accumulation over the past 1000 years, Clim. Past, 13, 1491–1513. https://doi.org/10.5194/cp-13-1491-2017, 2017.

Viale, M., & Garreaud, R. Summer precipitation events over the western slope of the subtropical Andes. Monthly Weather Review, 142(3), 1074-1092. https://doi.org/10.1175/MWR-D-13-00259.1, 2014.

Viale, M., Bianchi, E., Cara, L., Ruiz, L. E., Villalba, R., Pitte, P., Masiokas, M., Rivera, J., & Zalazar, L. Contrasting climates at both sides of the Andes in Argentina and Chile. Frontiers in Environmental Science, 7, 69. https://doi.org/10.3389/fenvs.2019.00069, 2019.

Wilks, D. S. Statistical Methods in the Atmospheric Sciences, Fourth Edition. In Statistical Methods in the Atmospheric Sciences, Fourth Edition. https://doi.org/10.1016/C2017-0-03921-6, 2019.